RSC Advances

PAPER

View Article Online
View Journal | View Issue

Open Access Article. Published on 13 February 2017. Downloaded on 5/9/2026 3:33:49 PM.
This article is licensed under a Creative Commons Attribution-NonCommercial 3.0 Unported Licence.

Cite this: *RSC Adv.*, 2017, 7, 11211

Controlled synthesis and wastewater treatment of Ag_2O/TiO_2 modified chitosan-based photocatalytic film

Yilin Zhao, Chengran Tao, Gang Xiao and Haijia Su*

Received 24th November 2016
Accepted 6th February 2017

DOI: 10.1039/c6ra27295a

rsc.li/rsc-advances

A novel Ag_2O/TiO_2-modified chitosan-based photocatalytic film with high adsorption and photocatalytic activity was synthesized under simulated solar irradiation, based upon the coupling of the synergistic catalytic technique of nano Ag_2O/TiO_2 and membrane separation. XRD, XPS, FESEM, and TEM characterization results illustrated that the Ag_2O nanoparticles with a small size of 3–5 nm deposited on the surface of TiO_2. Subsequently, Ag_2O–TiO_2 nanoheterojunctions, as whole graft-structures, were coated on a chitosan-based polypropylene film. The as-synthesized photocatalytic film with a wide visible-light adsorption band and lower band gap of 2.4 eV enhanced the degradation ability for both ampicillin and methyl orange owing to the synergistic effect of AgO_2/TiO_2 nanoheterojunctions. Moreover, the photocatalytic film displayed excellent recycling properties for the degradation of methyl orange by being reused for 5 times without losing its photocatalytic activity.

1. Introduction

Persistent organic pollutants (POPs) are causing concerned among the scientific community due to their persistence in the environment.[1] The photocatalytic process of nano TiO_2 has shown tremendous potential as a high-efficiency, low-cost, high physical-chemical stable and environmentally friendly technology to degrade POPs in wastewater.[2,3] Under ultraviolet (UV) light irradiation, electrons are emitted from TiO_2 inducing electron–hole pair formation, and subsequent charge separation induces the production of highly reactive oxygen species that can completely mineralize POPs. However, TiO_2 only responds to UV light with a wavelength below 387 nm.[4] This drawback limits the possibility of employing sunlight as a light source because UV light occupies fewer proportions (4%) of the sun's radiation energy than that of visible light (43%). In addition, high recombination rates, about 10 ns between electron and hole pairs, reduce the quantum yield of a single TiO_2 semiconductor.[5]

In order to improve the photocatalytic activity and visible light utilization of TiO_2, numerous studies, pertaining to the surface modification of TiO_2 nanoparticles with depositing noble metal NPs (Au, Ag, Pt, Pd, *etc.*),[6–10] and coupling with semiconductors, such as CdS,[11] Ag_2O,[12] V_2O_5,[13] WO_3 [14] and Bi_2O_3,[15] have been carried out and obtained excellent achievements. Compared with other metallics, Ag and Ag-based oxides are the most suitable for practical applications because of their relatively low-priced and high efficiency.[16] Ag_2O nanoparticles, a brown powder with a narrow band gap of 1.3 eV, are efficient electron absorbing agents under UV light irradiation and sensitizers to turn UV light response into the visible region.[17–19] Besides, Ag_2O has been used in various fields, as a mild oxidant, water cleaning agent, and catalyst.[20] The advantages of Ag_2O impel a novel strategy of combining Ag_2O and TiO_2 for superior photocatalysts in the visible light region.

Another main drawback of using nanosized TiO_2 is its complicated subsequent separation from water.[21] To handle this problem, various materials, such as glass,[22] stainless steel mesh,[23] fiber,[24] silica gel[25] and polymeric materials,[26] have been explored as a TiO_2 support for the photodegradation of contaminants in wastewater. Coupling nano-TiO_2 with organic polymers to fabricate membrane/globular composites is an efficient way for immobilization. Chitosan (CS) is the second most abundant natural polymer obtained from the cell walls of fungi and the shells of crust. CS has drawn a great attention for its excellent properties, such as blood compatibility, microbial degradation and environmental security.[27] Using chitosan as a carrier for TiO_2, chitosan-supported TiO_2 (CS–TiO_2) adsorbent was prepared and exhibited multifunctional performance for increasing the adsorption capacity of heavy metals and enhancing the adsorption–photocatalytic process of organic pollutants.[28] As a result, two forms of CS–TiO_2 composites were prepared: membrane and beads. Although globular resins can effectively degrade contaminants, the photocatalytic efficiency of CS–TiO_2 beads is usually lower than that of membrane systems due to the limited contact area with contaminants. It is highly desirable to develop membrane CS–TiO_2 composites with a better photocatalytic ability.

Beijing Key Laboratory of Bioprocess, Beijing University of Chemical Technology, Beijing 100029, PR China. E-mail: suhj@mail.buct.edu.cn; Fax: +86-10-64414268; Tel: +86-10-64452756

Open Access Article. Published on 13 February 2017. Downloaded on 5/9/2026 3:33:49 PM.
This article is licensed under a Creative Commons Attribution-NonCommercial 3.0 Unported Licence.

Based on the potential synergistic effects of Ag_2O and TiO_2, a new multilayer photocatalytic-membrane was fabricated, consisting of a Ag_2O/TiO_2 layer stacked on a chitosan sub-layer immobilized onto a polypropylene fiber substrate. FESEM, EDX, XRD, HRTEM, XPS, and UV-vis spectroscopy were used to characterize the films. The photocatalytic performance of Ag_2O/TiO_2-modified chitosan-based photocatalytic film (ATCPF) was analyzed by the degradation of ampicillin (AMP) and methyl orange (MO) with visible light irradiation. Chitosan-supported TiO_2 photocatalytic film (CTPF) was also prepared and its photocatalytic performance was evaluated with two model pollutants as reference. The reuse property of the obtained ATCPF was tested for a better understanding of its potential capability for practical applications. The present study developed an efficient photocatalyst towards organic pollutants and provided novel design ideas for effective visible-light-mediated nanocomposites photocatalysts.

2. Experimental section

2.1 Chemicals

Hydrophilic polypropylene fiber was purchased from Hengyue Nonwovens Company. Chitosan (90% degree of deacetylation) was bought from Jinan Haidebei Marine Bioengineering Co. Ltd. Nanosized bicrystalline TiO_2 (P25, 50 $m^2\ g^{-1}$, average particle size 30 nm) was purchased from Degussa. Sodium ampicillin (AMP) was bought from Sigma Aldrich (CAS: 69-52-3). Other chemicals were obtained from Beijing Chemical Plant, including ammonium hydroxide (NH_4OH), silver nitrate ($AgNO_3$), methyl orange (MO), acetic acid (CH_3COOH), epichlorohydrin (C_3H_5OCl) and sodium hydroxide (NaOH). All chemicals were of analytical grade, and used without further purification.

2.2 Sample preparation

2.2.1. Synthesis of chitosan/polypropylene film (CPF). (i) The polypropylene fiber was shaken in a 2.5% NaOH aqueous solution for 24 h to complete basification, followed by a drying process at room temperature. (ii) 0.1 g CS was dissolved into 10 mL 2.5% CH_3COOH liquid and dispersed with 100 W ultrasound for 15 min. Then, 1 mL epichlorohydrin (cross-linking agent) was added and stirred constantly for 4 h at 25 °C. (iii) The emulsion was dripped on the polypropylene film to fully cover it. By naturally drying the wet chitosan/polypropylene fiber, CP with a smooth surface was obtained.

2.2.2. Synthesis of Ag_2O/TiO_2-modified chitosan-based photocatalytic film (ATCPF). (i) 0.1 g TiO_2 nanoparticles were dispersed in 20 mL of 10 mM $AgNO_3$ aqueous solution. (ii) NH_4OH was dripped into the above TiO_2–$AgNO_3$ mixture solution to adjust the pH between 10 and 11, followed by photodeposition under 365 nm UV lamp (GE, 20 W) and vigorously stirring for 2 h. (iii) After switching off the UV lamp, CPF was impregnated into the solution for reacting another 5 h with a stirring rate of 100 rpm in the dark. Finally, ATCPF was neutralized and rinsed with deionized water when semi-damp, and then vacuum-dried at 40 °C. TiO_2-modified chitosan-based photocatalytic film (TCPF), Ag_2O/TiO_2 nanocomposites (AT) were also prepared as control.

2.3 Characterization

The morphology of ATCPF was observed by a FE-SEM (Hitachi S-4700, Tokyo, Japan) and a HRTEM (JOEL JEM 3010, Tokyo, Japan). The crystalline phase contained in TiO_2 and Ag_2O/TiO_2 was observed by XRD patterns in a Rigaku D/Max 2400 diffraction meter (Tokyo, Japan). XPS was recorded with the ESCALAB 250 system (Thermo Fisher Scientific, USA). UV-vis diffuse reflectance spectra were conducted on a UV-vis spectrophotometer (UV-3150, Shimadzu, Japan) attached with integrating sphere. All samples (5 mL) were filtrated with a 0.45 μm filter to remove COD and nitrogen, subsequently quantified the major cationic contents (Ti^{4+} and Ag^+ ions) by an Agilent 7700x ICP-MS (Agilent technologies, USA).

2.4 Photocatalytic activity

The photocatalytic performance of the samples was evaluated by degrading two organic compounds: MO and AMP Photochemical experiments were accomplished in a photocatalytic reaction chamber provided with one 150 W tungsten–halogen lamp that facilitated continuous emission of UV-visible light (λ = 360–2000 nm). Reactions were performed in a commercially available dish with a diameter of 90 mm. In a typical photocatalytic experiment, photocatalytic film with a diameter of 80 mm was dispersed into 40 mL MO (10 mg L^{-1}) solution or 40 mL AMP (20 mg L^{-1}) solution with constant stirring. Here, each piece of ATCPF or TCP was coated with 60 mg loading mass of catalysts (Ag_2O/TiO_2 or TiO_2).

The residual concentrations of MO were detected by UV-vis spectrophotometry (Varian, Cary100) at the wavelength of 464 nm. The degradation of AMP was detected by HPLC analysis with a C_{18} (5 μm, 4.6 mm × 150 mm) column at the wavelength of 220 nm. The degradation rate of MO and AMP could be calculated by eqn (1):

$$\text{Degradation rate }(\%) = \frac{C_0 - C_t}{C_0} \times 100\% \qquad (1)$$

where C_0 and C_t are the initial and final concentration (mg L^{-1}), respectively.

The antibacterial effect of the samples was analyzed by antibacterial tests and Disk Diffusion Assays using the method introduced by M. J. Umapathy.[6,29]

3. Results and discussion

3.1 Characterization of the prepared composite photocatalysts

3.1.1. Morphological investigation with SEM, EDS and TEM. The FE-SEMs of these samples were shown in Fig. 1. Compared to pristine polypropylene fiber (Fig. 1a), both the surface and gap of blank fiber were covered by smooth films, indicating good viscosity stability and film-forming properties of the chitosan/acetic acid solution (Fig. 1b). TiO_2 nanoparticles were evenly coated on the surface of the CP after synthesizing

Open Access Article. Published on 13 February 2017. Downloaded on 5/9/2026 3:33:49 PM.
This article is licensed under a Creative Commons Attribution-NonCommercial 3.0 Unported Licence.

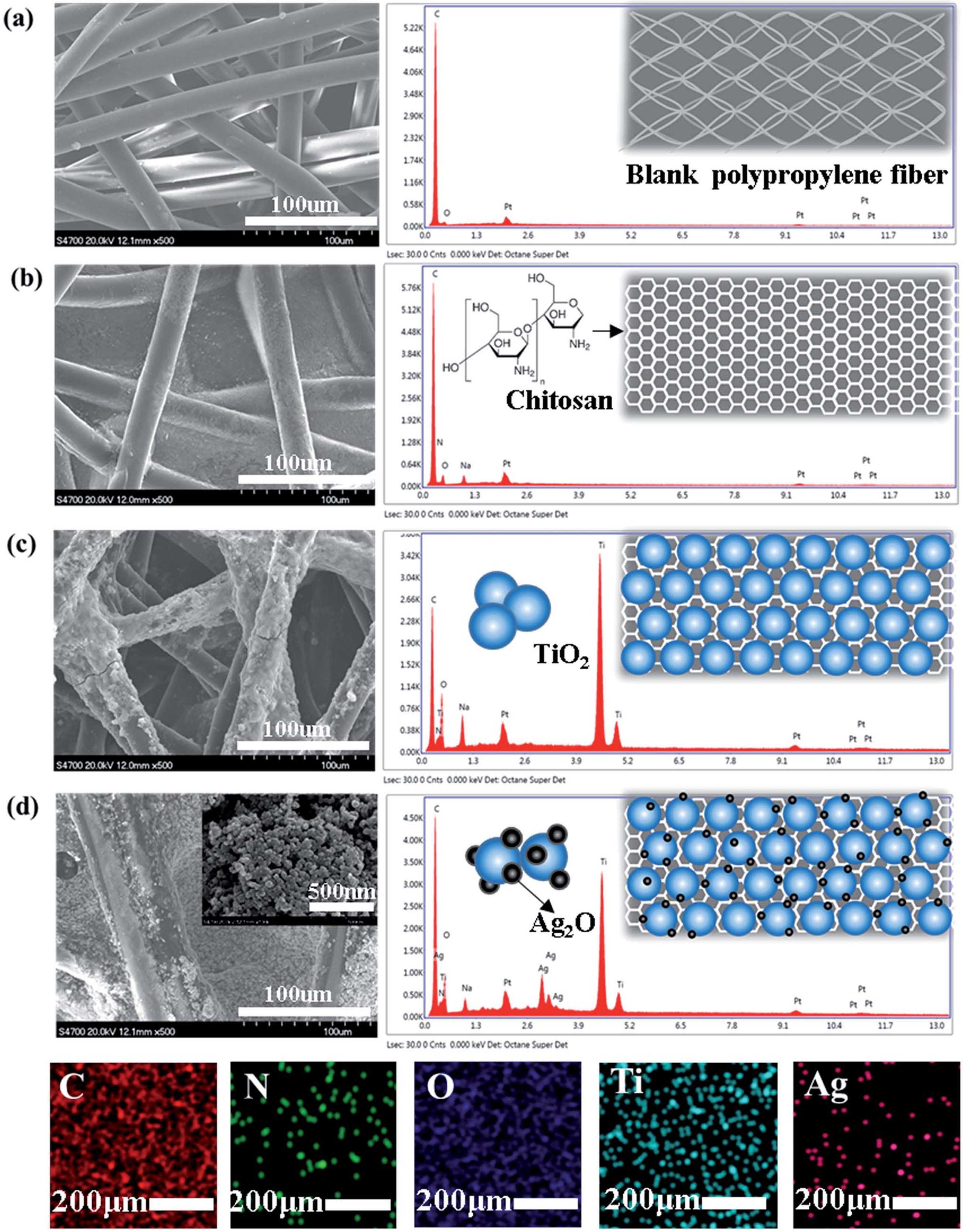

Fig. 1 SEM images and EDX spectrum of (a) blank polypropylene fiber; (b) CPF; (c) TCPF (d) ATCPF with different magnifications.

Open Access Article. Published on 13 February 2017. Downloaded on 5/9/2026 3:33:49 PM.
This article is licensed under a Creative Commons Attribution-NonCommercial 3.0 Unported Licence.

TCP (Fig. 1c). When Ag_2O/TiO_2 had been deposited on CP (Fig. 1d), a rough surface coated with homogeneous granulation was developed. With the 500× magnification, obvious nanoclusters were revealed and illustrated in Fig. 1d (inset), from which the particle size of aggregated Ag_2O/TiO_2 was measured in the range of 50–500 nm. It was the result of nanoparticle aggregation at high TiO_2-NPs content during the preparation. With the even coverage of polypropylene fiber by chitosan, the chitosan/polypropylene fiber composites (CP) provided a platform with high surface area for adhesion of Ag_2O/TiO_2.

Surface elemental analysis containing EDX spectrum has been done and the results are shown in Fig. 1 respectively. TCP shows more distinct elemental peaks of Ti and ATCPF shows more distinct elemental peaks of Ag and Ti than that of CP. Different color areas shown in Fig. 1d indicate C-, N-, O-, Ti and Ag-enriched areas of ATCPF. It revealed that the obtained film was composited of the elements of C, N, O, Ti and Ag, and also showed the homogeneous distribution of the Ag ions on the surface. The peaks of C element mainly resulted from the polypropylene film, while the peak of N element resulted from chitosan. The results demonstrated high-density TiO_2 and Ag_2O had been immobilized on the surface of the heterozygous nanocomposites.

In order to further confirm the distribution of both TiO_2 and Ag, morphology details of the ATCPF were analyzed by HRTEM. Dispersed Ag_2O nanoparticles were tightly coupled onto the surface of TiO_2 with an average diameter of 3–5 nm (Fig. 2a). The resolved interplanar distances was 0.27 nm, corresponding to the (111) plane of Ag_2O (Fig. 2b). On the basis of the SEM and TEM observation, a schematic structure of the ATCP was depicted in Fig. 2c. In the alkaline $AgNO_3$ solution, Ag^+ was firstly adsorbed to the surface of TiO_2 and then transformed into Ag_2O under UV light illumination. The subsequent addition of chitosan/polypropylene fiber provided an excellent-carrier for the nanocrystals loading. As a result, Ag_2O/TiO_2 was deposited on the chitosan-modified polypropylene fiber, making the white fiber color purple-black. Our earlier study of FT-IR[30] indicated that the hydrogen bonding interaction was a main driving force for the self-assembly between TiO_2 with surface hydroxyl group and chitosan with amino and hydroxyl. Similarly, Ag_2O-modified TiO_2 also could easily combine with chitosan/polypropylene fiber *via* hydrogen bonding interaction. On the basis of the formation mechanism, ATCPF with a graft-like structure had been synthesized, and shown appropriate for follow-up application.

3.1.2. **Elemental compositions analysis.** To prove the synthesis of ATCPF, the crystal structures and chemical status of these samples were analyzed. XRD patterns of TCP and ATCPF were shown in Fig. 3a. The XRD pattern of TCP displayed that TiO_2 has a bicrystalline structure, which can be assigned to anatase and rutile phases. After coating with Ag nanoparticles, ATCPF showed additional peaks when compared with TCPF.

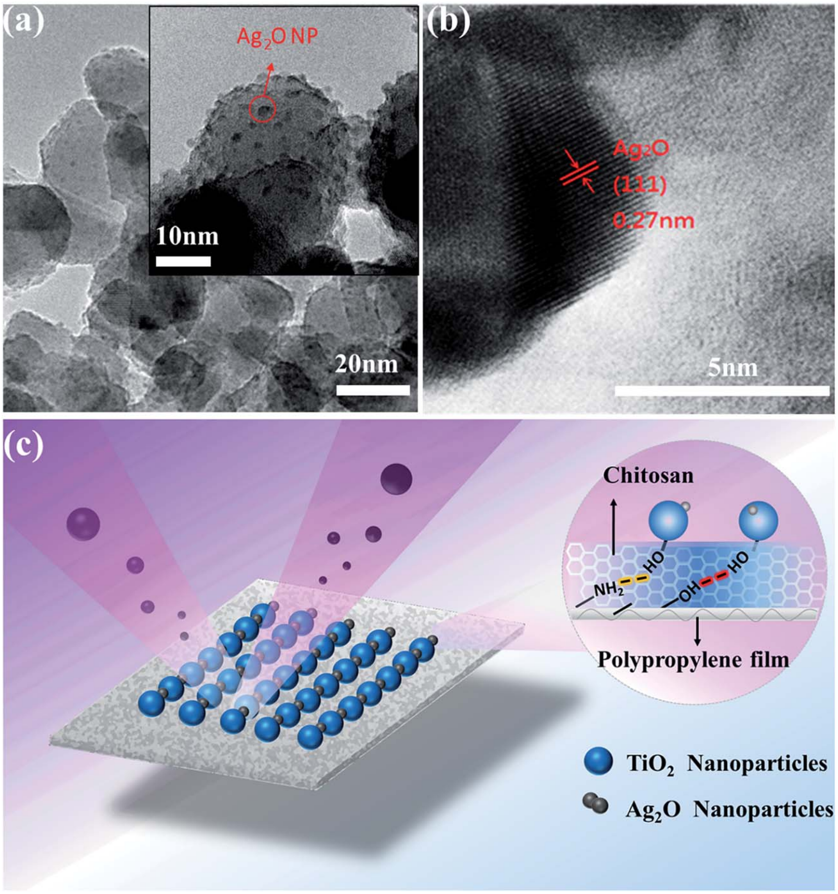

Fig. 2 (a and b) HRTEM image and (c) schematic structure of the ATCPF.

Open Access Article. Published on 13 February 2017. Downloaded on 5/9/2026 3:33:49 PM.
This article is licensed under a Creative Commons Attribution-NonCommercial 3.0 Unported Licence.

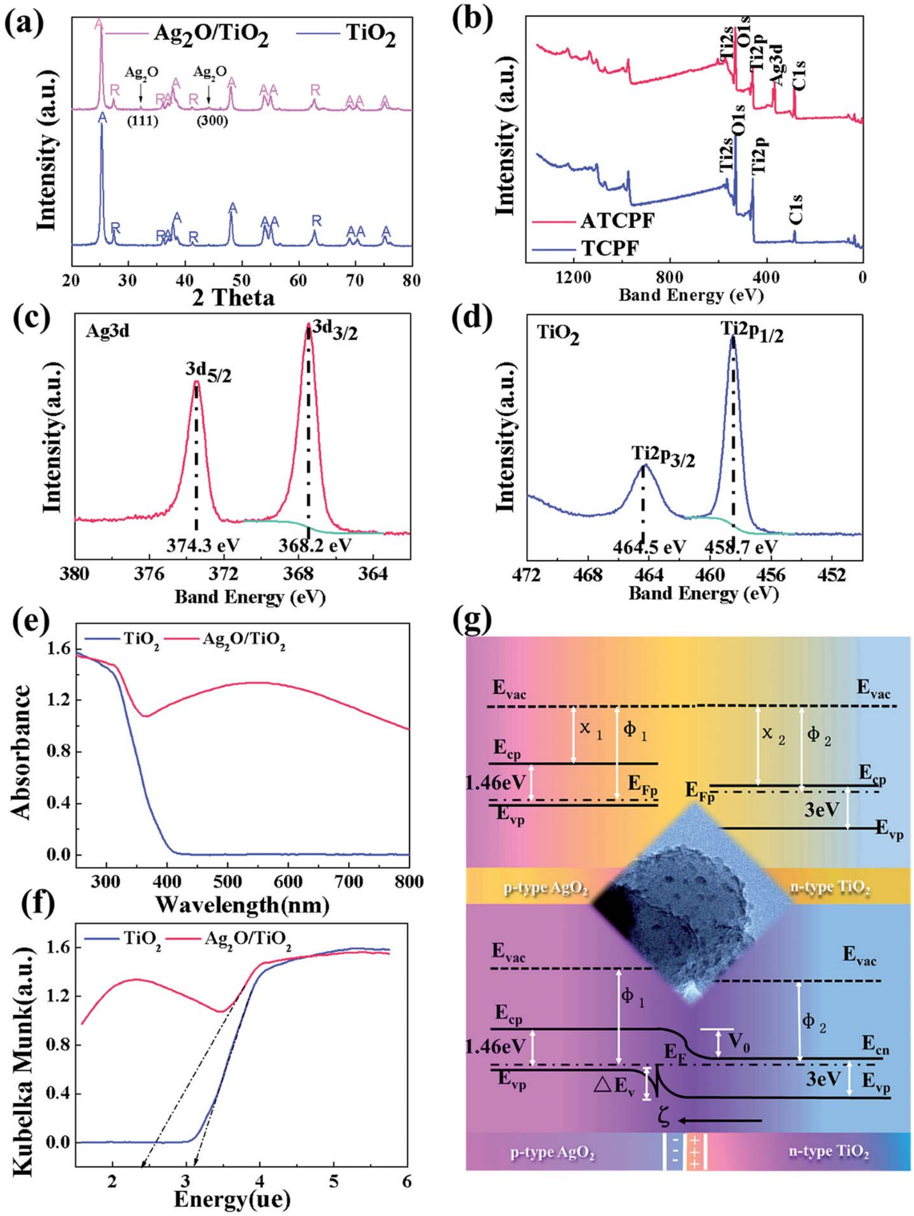

Fig. 3 (a) XRD pattern of TiO_2 and Ag_2O/TiO_2 scraped off from ATCPF (A: anatase, R: rutile). (b) XPS survey scan spectra of pure TiO_2 and Ag_2O/TiO_2; (c) XPS spectra for Ag $3d_{5/2}$ and $3d_{3/2}$; (d) XPS spectra for TiO_2 $2P_{3/2}$ and $2P_{1/2}$; (e) UV-vis absorption spectra of Ag_2O/TiO_2 and TiO_2; (f) the band-gap energies of ATCPF and TCPF; (g) the energy band structure of Ag_2O and TiO_2 before contact and the energy band structure of p-Ag_2O/n-TiO_2 heterojunction at equilibrium (E_{vac}: vacuum level; E_F: Fermi level; ϕ: work function; χ: electron affinity).

Two obvious peaks for Ag_2O were detected at 32.8° {111} (JCPDS no. 41-1104) and 46.14° {300} (JCPDS no. 42-0874), which demonstrates that the Ag_2O nanoparticles are coated on the surface of TCP but not inserted in the crystal lattice.

The elemental compositions and chemical status of TCPF and ATCPF were characterized by XPS (Fig. 3b–d). Compared with TCP, additional peaks of Ag were found in ATCPF in addition to the Ti, O, and C peaks (Fig. 3b). High-resolution scan over Ag $3d_{5/2}$ in Ag_2O/TiO_2 nanoparticles demonstrated that the binding energy is 367.47 eV, which is consistent with values reported for Ag_2O.[30] Meanwhile, the signals of Ti $2p_{3/2}$ and Ti $2p_{1/2}$ at ~458 eV and ~464 eV corresponding to TiO_2 (Fig. 3d).[31] It indicated that silver existed in only one valence state (Ag^+) as Ag_2O in the obtained mixture. Therefore, the nanoparticles scraped from ATCPF confirmed that TiO_2 nanoparticles were successfully modified by Ag_2O based on XRD and XPS characterization.

3.1.3. Mechanism of photocatalytic activity. The UV-vis diffuse reflectance spectra for TCP and ATCPF are shown in Fig. 3e. A broad intense adsorption of TCPF is in the UV region below 400 nm; however, a strong and wide adsorption of ATCPF is in the visible-light region at 545 nm with maximum. The band-gap energy of TCPF is 3.1 eV and the band-gap energy of ATCPF presents a marked displacement to lower energy values

Open Access Article. Published on 13 February 2017. Downloaded on 5/9/2026 3:33:49 PM. This article is licensed under a Creative Commons Attribution-NonCommercial 3.0 Unported Licence.

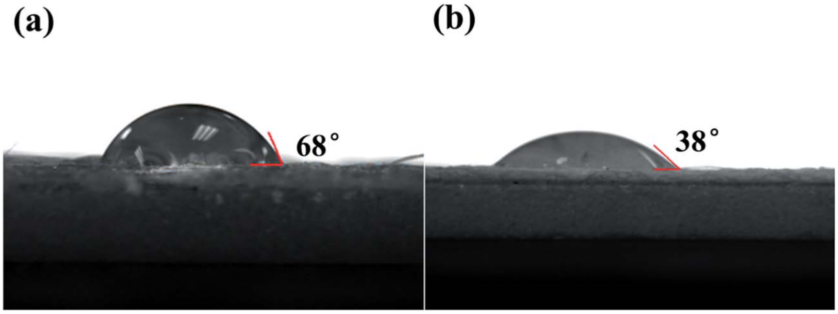

Fig. 4 Contact angle characterization of (a) blank film and (b) ATCPF.

at 2.4 eV approximately, which were estimated by the Kubelka–Munk method (Fig. 3f).[32] The wide visible light adsorption and low band gap in ATCPF nanocluster are all owe to the formation of p–n heterojunctions as visible-light sensitization. Ag_2O is a p-type narrow band gap semiconductor, while TiO_2 is an n-type wide band gap semiconductor. As shown in Fig. 3g, p–n heterojunctions are synthesised at the interface and electron transfer occurred from TiO_2 to Ag_2O when their Fermi levels align. At the equilibrium of junction, the charge of n-type TiO_2 regions is positive, while the charge of p-type Ag_2O is negative. Therefore, an opposing electric field (ξ, contact potential) at the junction and an equilibrium potential difference V_0 are formed across the transition region. During the photocatalytic reaction process of p-Ag_2O/n-TiO_2 nanojunction, the photogenerated electrons move to the conduction band (E_{cn}) of the n-type TiO_2 and holes move to the valence band (E_{vp}) of the p-type Ag_2O. The charge separation (e^-/h^+) were effectively by trapping photoelectrons on Ag_2O nanoparticles and powerful oxidizing agent and superoxide radical (OH^-, O^{2-}, $^{\bullet}OOH$, $^{\bullet}OH$) were produced subsequently in a photocatalysis degradation reaction.

3.1.4. Water contact angle measurement. In order to understand the surface hydrophilic for photocatalysis degradation and self-cleaning application, water contact angle of samples was analyzed. As shown in Fig. 4, the water contact angle of the bare substrate is 68°; however, the contact angle of the ATCPF is only 38°. The result demonstrated that hydrophilicity of the film tends to increase after modifying. A plausible mechanism for this phenomenon have been suggested that both chitosan and TiO_2 are abundant hydrophilic group, for example, $^{\bullet}OH$. In water treatment, the good hydrophilicity of ATCPF is conducive to water molecule diffusion and mass transfer, and it is easy to combine and degrade pollutant.

3.2 Photocatalytic activities

To probe advantages of ATCPF, adsorbing capacity and degradation experiments were carried out by adsorbing and decomposing typical compounds: AMP and MO. These two typical compounds were chosen as model organic pollutants because antibiotic and azo dyes both involve serious risks for the human being and aquatic environment.

3.2.1. Adsorption and degradation of ampicillin (AMP). As shown in Fig. 5a, in the dark, ATCPF was more efficient in reducing the concentration of AMP than TCPF, CPF and AT, which indicated that the surface adsorption properties of ATCPF had been obvious increased when TCPF was modified by Ag_2O. Chitosan had no apparent adsorption effect on AMP, which was probably due to the steric macromolecular hindrance between chitosan and AMP. As shown in Fig. 5b, ATCPF exhibited the highest photocatalytic activity of MO degradation under simulated solar irradiation, the following series of photoactivity were found: ATCPF > AT > TCPF > CPF polypropylene film. It was clear that the removal of AMP by blank polypropylene fiber, CPF and AT were all depressed, which meant that AMP cannot be degraded directly by blank film or chitosan. In the case of the TCPF and AT, the

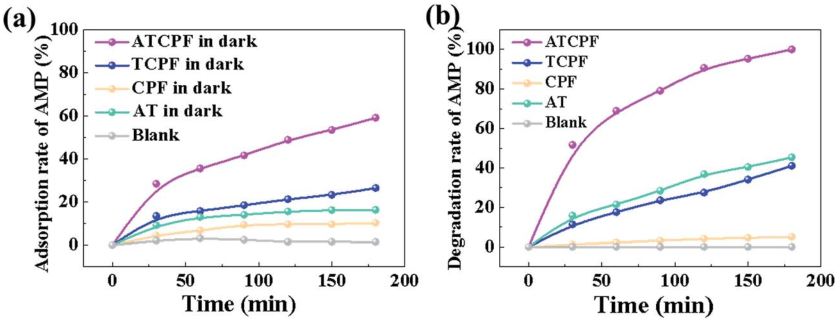

Fig. 5 (a) The adsorption of AMP in dark condition within the presence of ATCPF, TCPF, CPF, AT nanoparticles and blank polypropylene film; (b) the degradation of AMP (20 mg L^{-1}, 40 mL) during simulated solar irradiation in the presence of ATCPF, TCPF, CPF, Ag_2O/TiO_2 nanocomposites (AT) and blank polypropylene film.

Open Access Article. Published on 13 February 2017. Downloaded on 5/9/2026 3:33:49 PM.
This article is licensed under a Creative Commons Attribution-NonCommercial 3.0 Unported Licence.

concentration of AMP continued to decline as the irradiation time was prolonged; however, only about 40% of AMP was degraded within 3 h in the presence of TCP or AT. In comparison, ATCPF exhibited a considerable degradation ability of AMP under simulated solar irradiation, and the degradation rate of AMP reached 100% in 3 h. Compared with CPF, the distinguished performance of ATCPF should be attributed to the graft structure of Ag_2O/TiO_2 heterostructures, which expose to contact AMP in the solution and induce photocatalytic oxidation reaction. Combining CPF with Ag_2O/TiO_2 by self-assembly to form ATCPF also prevented the interference of chitosan to AMP, which was in good agreement with the schematic structure (Fig. 2c). The degradation activity of ATCPF under simulated solar irradiation was much higher than the dark case, and the corresponding removal rate was 59.2% after 3 h. Although ATCPF plays an important role in reducing AMP without irradiation, the light treatment was considered necessary to improve the photocatalytic performance of ATCPF.

3.2.2. Degradation of MO.

To further evaluate the multifunctionality of ATCPF, the adsorption and decomposition of MO were examined, as shown in Fig. 6. In the dark condition, ATCPF still performed good decolorization of MO. It was found that blank polypropylene film and AT again had no effect on MO, whereas CPF possessed absorptivity and reached saturation about 34.6% in 15 min. This phenomenon was slightly different from the case of AMP, which was due to the interaction between the functional groups (hydroxyl and amine) of chitosan and MO.[33] After the surface of CPF was coated with TiO_2, the obtained TCPF exhibited a slightly stronger adsorption capacity of MO in the dark, and about 50.3% decolorization was attained, indicating that TiO_2 also had affinity for MO owing to the hydroxyl groups on the surface of TiO_2.[34] When exposed to visible light, photocatalytic activity of TCP was more efficient than that of CP. It could be attributed to both the adsorption of CPF and photocatalysis of AT under simulated solar irradiation. Similar to the case of ATCPF for degrading AMP, the photocatalysis degradation of MO by ATCPF occurred at a significantly higher rate than that by TCPF, thoroughly completed within 30 min under visible light irradiation. The above results further indicated that the as-prepared ATCPF can be used as a highly efficient photocatalyst that can use simulated sunlight.

3.2.3. Comparison of reaction rate constant of ATCPF and TCPF.

The reaction rate constants (k) of ATCPF and TCPF were analyzed by re-plotting the degradation rate of AMP and MO according to the following equation:

$$-\frac{\mathrm{d}C}{\mathrm{d}t} = kC$$

As shown in Table 1, during the degradation process of AMP and MO under simulated solar irradiation, the values of k indicated that the rate constant of ATCPF was much faster than that of TCP, CPF and AT. The photocatalysis mechanisms of ATCPF under UV- and visible-light irradiation are different. In the UV range, both TiO_2 and Ag_2O are excited to produced electron–hole pairs, and then the generated electrons and holes can react with H_2O to produce powerful oxidizing agent and superoxide radical.[35] In the visible range, only Ag_2O can be excited to produce electron–hole pairs, which then act as visible-light active component to enhance the Ag_2O/TiO_2 photocatalytic activity to decompose organic pollutants. Therefore, these two different mechanisms under UV-visible light jointly promoted the photocatalytic process of ATCPF.

3.2.4. Mineralization studies.

The mineralization effects were analyzed by studying the TOC contents of reaction solution during photocatalytic reaction. After reaction with ATCPF for 15 min, the degradation rate of MO was 96.00% and the removal rate of TOC was 83.77% (Fig. 7a). It demonstrated that mineralization is a synchronously process with degradation reaction. The results further indicated that the as-prepared ATCPF can be used as a highly efficient mineralization photocatalyst that can mineralize dye efficiently with simulated sunlight. However, as shown in Fig. 7b, after reaction with TCPF for 15 min, the degradation rate of MO was 73.41%, while the TOC removal rate was only 24.75%. The results demonstrated that the mineralization process was significantly improved because of the excellent photocatalysis of Ag_2O.

3.2.5. Photocatalytic antibacterial characteristics.

To evaluate the antibacterial activity of the Ag_2O/TiO_2 modified chitosan-based photocatalytic film, the bactericidal efficiency of ATCPF was compared to the activities of the other photocatalysts materials. As shown in Fig. 8a, a negligible

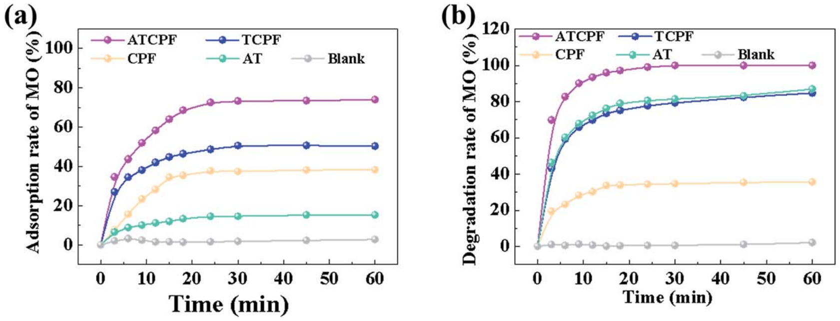

Fig. 6 (a) The adsorption of MO (10 mg L^{-1}, 40 mL) in dark condition within the presence of ATCPF, TCPF, CPF, AT and blank film polypropylene. (b) The degradation of MO (10 mg L^{-1}, 40 mL) during simulated solar irradiation in the presence of ATCPF, TCPF, CPF, AT and blank polypropylene film.

Open Access Article. Published on 13 February 2017. Downloaded on 5/9/2026 3:33:49 PM. This article is licensed under a Creative Commons Attribution-NonCommercial 3.0 Unported Licence.

Table 1 The rate constant during photocatalytic degradation of AMP and MO

Pollutants systems (under simulated solar irradiation)	k_{ATCPF} ($\times 10^{-4}$ min^{-1})	k_{TCPF} ($\times 10^{-4}$ min^{-1})	k_{CPF} ($\times 10^{-4}$ min^{-1})	k_{AT} ($\times 10^{-4}$ min^{-1})
AMP ($C_0 = 20$ mg L^{-1})	196	27	0.11	38
MO ($C_0 = 10$ mg L^{-1})	164	32	14	89

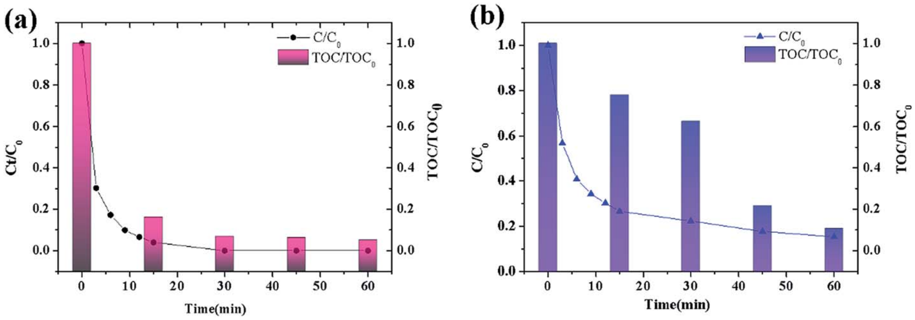

Fig. 7 Concentration change and TOC analysis of (a) ATCPF, (b) TCPF during photocatalytic degradation of MO ($C_{0\ MO} = 10$ mg L^{-1}; $V = 40$ mL; $M = 0.075$ g; $N = 70$ rpm; UV; $t = 6$ h).

antibacterial activity was observed in the absence of photocatalyst (curve 1). Because of the lower photocatalytic activity of AT and CPF under visible light, only 56% and 35% inactivation of *E. coli* was found even after 60 min of irradiation (curve 3 and 4). In contrast, obvious enhancements in visible-light bactericidal efficiency was observed on TCPF (curve 5) and ATCPF (curve 6). In particular, ~99.8% of the *E. coli* was killed on the ATCPF upon irradiation for 60 min (curve 6). Additionally, by comparing the bactericidal results on ATCPF in the presence (curve 6) and absence (curve 2) of visible-light irradiation, it is obvious that, apart from the effect of the Ag^+ ions, the mainly bactericidal effects is related to the photocatalytic process. As shown in Fig. 8b, the antibacterial activity of ATCPF was also assessed by the diameter of inhibition zone (DIZ) test with various concentrations of *E. coil*. From the results of DIZ test under visible light (Fig. 8c), it was observed that PF, CPF and TCPF did not show any antimicrobial activities by visible light; however, ATCPF showed a palpable DIZ value which indicating significant antibacterial activity against *E. coli* with a concentrations of approximately 10^4 CFU mL^{-1}. It can be predicted that the excellent biocidal function of ATCPF is derived from the Ag species and the oxidative stress caused by photo-generated reactive radicals.[6,29]

3.2.6. **Multiple reuse ability.** To investigate the stability of ATCPF on the photocatalytic activity under simulated solar irradiation, the same samples were reused for five times to remove MO, and results were shown in Fig. 9. For comparison, the repeated degradation experiments were also carried out in the dark condition. Under irradiation, it was found that MO can be fully degraded within 30 min in the first two cycles. Along

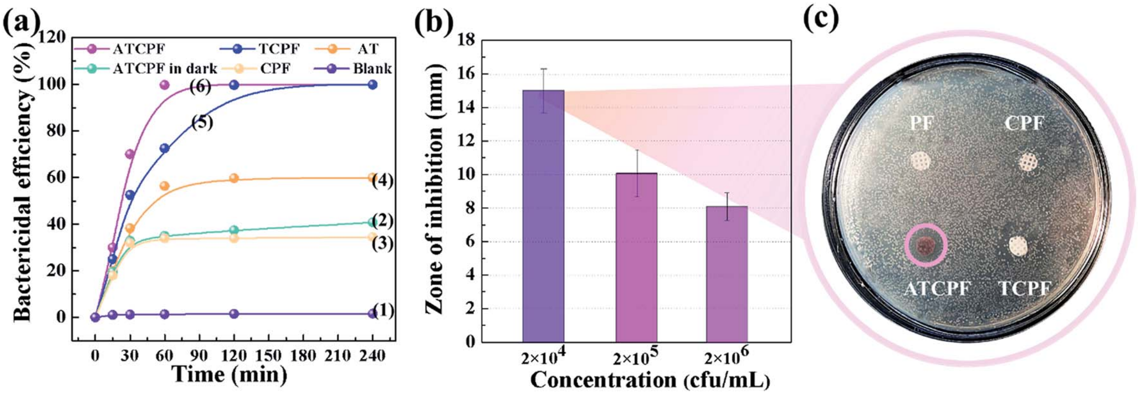

Fig. 8 (a) Kinetics of bactericidal efficiency against *E. coli* under visible-light irradiation: (1) *E. coli* suspension without any catalyst irradiated by visible light, (2) *E. coli* suspensions with 0.1 g of ATCPF in the dark, (3–6) *E. coli* suspensions with 0.1 g of (3) CPF, (4) AT, (5) CTPF and (6) ACTPF. (b) Comparative study of the zone of inhibition (mm) for ATCPF in *E. coli* bacterial strain under visible-light irradiation. (c) Photographs of antibacterial results on *E. coli* for ATCPF.

Open Access Article. Published on 13 February 2017. Downloaded on 5/9/2026 3:33:49 PM. This article is licensed under a Creative Commons Attribution-NonCommercial 3.0 Unported Licence.

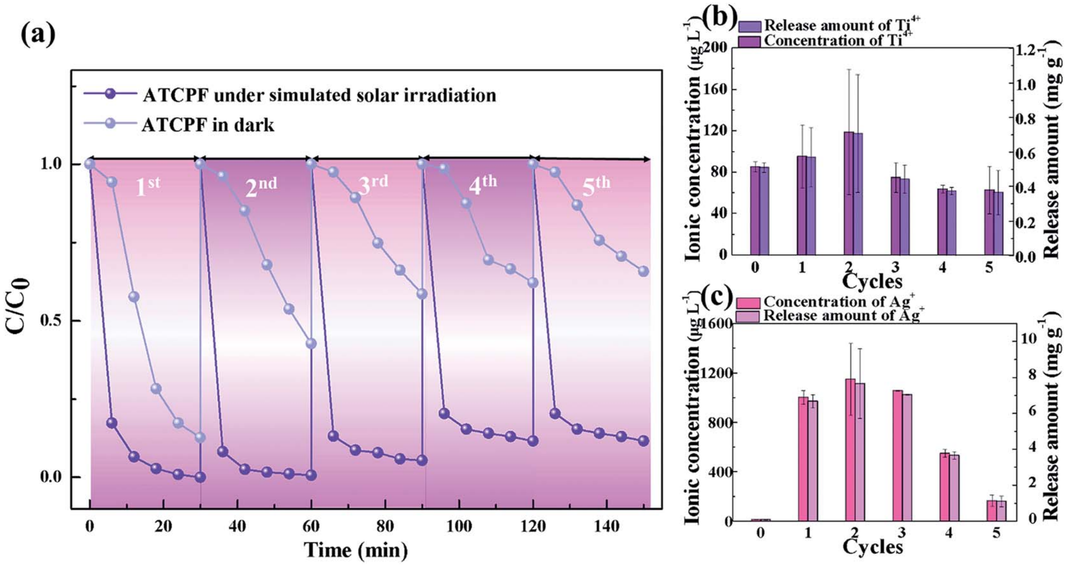

Fig. 9 (a) Repeated adsorption–photocatalytic degradation experiments carried out under simulated solar irradiation and in dark showing the photodegradation efficiency and recyclability of ATCPF composites in the degradation of MO ($C_0 = 10$ mg L^{-1}, $V = 40$ mL). (b and c) Ionic concentration and release amount of Ti^{4+} and Ag^+ during reused for five times.

with the increase of reusing times, the photocatalytic efficiency of ATCPF decreases slightly. This might be because of the presumed loss of Ag_2O/TiO_2 nanoparticles or because of some degradation intermediates that cover the surface of the as-prepared samples. Nevertheless, the degradation rate of MO still remains over 90% after reusing 5 times. However, in the case of dark application, the degradation efficiency of ATCPF severely diminishes with the increase of repeated use. Once reaching adsorption equilibrium, the concentration of MO would no longer decrease. Therefore, irradiation seems to be necessary to keep the high photocatalytic activity and stability of ATCPF. In addition, ATCP can be easily separated and reused directly without extra regeneration processes.

The possible release amount of Ag ion and Ti ion in the solution after ATCPF was reused different times were determined by ICP-MS, and the results are shown in Fig. 9b and c. Compared with control group, a negligible concentration of Ti^{4+} was detected during reused for five times, which demonstrated that TiO_2 nanoparticles were modified on the surface of CPF firmly. While about 1 mg L^{-1} Ag^+ was detected during former three times reusing. It can be predicted that the increase of released amount of Ag^+ led to the decrease of photocatalytic activity.

The observed adsorption performance, photocatalytic performance and stable reusability are far better than most of the reported nanostructures which has been summarized in

Table 2 Performance of photocatalytic activity in literature

Catalyst used and amount	Conc. and volume of MO	Light source (W)	Time (min)	Degradation (%)	Adsorption (%)	Repeated photooxidation (%)	Reference
Ag_2O/TiO_2 photocatalytic film (10 mg)	10 mg L^{-1}, 40 mL	150 (vis)	15	96	64	90 (5th)	Our work
Ag_2O/TiO_2 nanobelt (10 mg)	20 mg L^{-1}, 10 mL	350 (vis)	80	86	∼3	—	36
Ag_2O/TiO_2 nanobelts (20 mg)	20 mg L^{-1}, 20 mL	300 (vis)	25	80	—	76 (4th)	37
S-Doped Ag_2O/TiO_2 nanobelt (20 mg)	20 mg L^{-1}, 20 mL	300 (vis)	150	80	—	80 (6th)	38
Ag_2O/TiO_2 microsphere (20 mg)	14 mg L^{-1}, 50 mL	500 (vis)	60	99	—	—	39
Ag_2O/TiO_2 nanosheet (100 mg)	160 mg L^{-1}, 100 mL	160 (UV)	60	20	87.5	78 (5th)	40
Ag_2O nanocomposites (30 mg)	16 mg L^{-1}, 10 mL	500 (UV)	8	98	5	100 (8th)	41
Ag_2O/TiO_2 microspheres (40 mg)	∼3 mg L^{-1}, 40 mL	40 (UV)	15	93	∼3	93 (5th)	42

Open Access Article. Published on 13 February 2017. Downloaded on 5/9/2026 3:33:49 PM. This article is licensed under a Creative Commons Attribution-NonCommercial 3.0 Unported Licence.

Table 2. Therefore, the prepared ATCP can be regarded as a highly active, easily separated and highly stable sunlight photocatalyst, which shows a great potential in the field of environmental remediation through its simplicity and low-cost.

4. Conclusions

Based on the synergistic catalytic technique of Ag_2O and TiO_2 semiconductors, the sunlight active Ag_2O/TiO_2-modified chitosan-based photocatalytic film was successfully prepared. FESEM, HRTEM, XRD and XPS were used for the characterization of ATCPF, illustrating that Ag_2O nanoparticles were firstly deposited on TiO_2 nano-cluster and then Ag_2O/TiO_2 was as a whole immobilized on chitosan-modified polypropylene fiber, a multilayer composite with graft-like structure was obtained. The hydrophilic ATCPF film displayed excellent absorption capacity by modified chitosan, TiO_2 and Ag_2O. Because of its visible-light absorption and low band energy, the ATCPF film showed excellent photocatalytic property towards the complete degradation of two different target organics: AMP and MO, within 180 min and 30 min, respectively. ATCPF can be reused directly for 5 times with its photocatalytic efficiency for MO remaining in excess of 90%, which ensured a good stability and recyclability of the composite. The present study developed an efficient sunlight activated photocatalyst, and it is of realistic significance in wastewater treatment as well as scientific significance in designing visible light active nano-photocatalysts.

Acknowledgements

The authors express their thanks for the supports from the National Natural Science Foundation of China (21525625), the National Basic Research Program (973 Program) of China (2014CB745100), the (863) High Technology Project (2013AA020302) and the Chinese Universities Scientific Fund (JD1417).

References

1 R. Chalasani and S. Vasudevan, Cyclodextrin-functionalized Fe_3O_4@TiO_2: reusable, magnetic nanoparticles for photocatalytic degradation of endocrine-disrupting chemicals in water supplies, *ACS Nano*, 2013, 7, 4093–4104.

2 V. Vaiano, O. Sacco, D. Sannino and P. Ciambelli, Nanostructured N-doped TiO_2 coated on glass spheres for the photocatalytic removal of organic dyes under UV or visible light irradiation, *Appl. Catal., B*, 2015, **170**, 153–161.

3 J. Zhang, W. Wu, S. Yan, G. Chu, S. Zhao, X. Wang and C. Li, Enhanced photocatalytic activity for the degradation of rhodamine B by TiO_2 modified with Gd_2O_3 calcined at high temperature, *Appl. Surf. Sci.*, 2015, **344**, 249–256.

4 E. Schüler, A. K Gustavsson, S. Hertenberger and K. Sattler, Solar photocatalytic and electrokinetic studies of TiO_2/Ag nanoparticle suspensions, *Sol. Energy*, 2013, **96**, 220–226.

5 N. Pugazhenthiran, S. Murugesan, P. Sathishkumar and S. Anandan, Photocatalytic degradation of ceftiofur sodium in the presence of gold nanoparticles loaded TiO_2 under UV-visible light, *Chem. Eng. J.*, 2014, **241**, 401–409.

6 G. Xiao, X. Zhang, W. Zhang, S. Zhang, H. Su and T. Tan, Visible-light-mediated synergistic photocatalytic antimicrobial effects and mechanism of Ag-nanoparticles@chitosan–TiO_2 organic–inorganic composites for water disinfection, *Appl. Catal., B*, 2015, **170**, 255–262.

7 M. M. Mohamed and M. S. Al-Sharif, Visible light assisted reduction of 4-nitrophenol to 4-aminophenol on Ag/TiO_2 photocatalysts synthesized by hybrid templates, *Appl. Catal., B*, 2013, **142**, 432–441.

8 L. Xiang, X. Zhao, C. Shang and J. Yin, Au or Ag nanoparticle-decorated 3D urchin-like TiO_2 nanostructures: synthesis, characterization, and enhanced photocatalytic activity, *J. Colloid Interface Sci.*, 2013, **403**, 22–28.

9 A. V. Rosario and E. C. Pereira, The role of Pt addition on the photocatalytic activity of TiO_2 nanoparticles: the limit between doping and metallization, *Appl. Catal., B*, 2014, **144**, 840–845.

10 R. Molinari, C. Lavorato and P. Argurio, Photocatalytic reduction of acetophenone in membrane reactors under UV and visible light using TiO_2 and Pd/TiO_2 catalysts, *Chem. Eng. J.*, 2015, **274**, 307–316.

11 M. Kim, Y. K. Kim, S. K. Lim, S. Kim and S. I. In, Efficient visible light-induced H_2 production by Au@CdS/TiO_2 nanofibers: Synergistic effect of core–shell structured Au@CdS and densely packed TiO_2 nanoparticles, *Appl. Catal., B*, 2015, **166**, 423–431.

12 W. Zhou, H. Liu, J. Wang, D. Liu, G. Du, S. Han, J. Lin and R. Wang, Interface dominated high photocatalytic properties of electrostatic self-assembled Ag_2O/TiO_2 heterostructure, *Phys. Chem. Chem. Phys.*, 2010, **12**, 15119–15123.

13 J. Lichtenberger and M. D. Amiridis, Catalytic oxidation of chlorinated benzenes over V_2O_5/TiO_2 catalysts, *J. Catal.*, 2004, **223**, 296–308.

14 T. Arai, M. Horiguchi, M. Yanagida, T. Gunji, H. Sugihara and K. Sayama, Reaction mechanism and activity of WO_3-catalyzed photodegradation of organic substances promoted by a CuO cocatalyst, *J. Phys. Chem. C*, 2009, **113**, 6602–6609.

15 Y. Huo, X. Chen, J. Zhang, G. Pan, J. Jia and H. Li, Ordered macroporous Bi_2O_3/TiO_2 film coated on a rotating disk with enhanced photocatalytic activity under visible irradiation, *Appl. Catal., B*, 2014, **148**, 550–556.

16 X. Wang, S. Li, H. Yu, H. Yu, J. Yu and S. Liu, Ag_2O as a New Visible-Light Photocatalyst: Self-Stability and High Photocatalytic Activity, *Chem.–Eur. J.*, 2011, **17**, 7777–7780.

17 G. Wang, X. Ma, B. Huang, H. Cheng, Z. Wang, J. Zhan, X. Qin, X. Zhang and Y. Dai, Controlled synthesis of Ag_2O microcrystals with facet-dependent photocatalytic activities, *J. Mater. Chem.*, 2012, **22**, 21189–21194.

18 M. Xu, L. Han and S. Dong, Facile fabrication of highly efficient g-C_3N_4/Ag_2O heterostructured photocatalysts with enhanced visible-light photocatalytic activity, *ACS Appl. Mater. Interfaces*, 2013, **5**, 12533–12540.

This journal is © The Royal Society of Chemistry 2017

Open Access Article. Published on 13 February 2017. Downloaded on 5/9/2026 3:33:49 PM. This article is licensed under a Creative Commons Attribution-NonCommercial 3.0 Unported Licence.

19 R. Liu, P. Wang, X. Wang, H. Yu and J. Yu, UV- and visible-light photocatalytic activity of simultaneously deposited and doped Ag/Ag(I)–TiO_2 photocatalyst, *J. Phys. Chem. C*, 2012, **116**, 17721–17728.

20 J. Zou, Y. Xu, B. Hou, D. Wu and Y. Sun, Self-assembly Ag_2O nanoparticles into nanowires with the aid of amino-functionalized silica nanoparticles, *Powder Technol.*, 2008, **183**, 122–126.

21 D. Li, H. Zheng, Q. Wang, X. Wang, W. Jiang, Z. Zhang and Y. Yang, A novel double-cylindrical-shell photoreactor immobilized with monolayer TiO_2-coated silica gel beads for photocatalytic degradation of rhodamine B and methyl orange in aqueous solution, *Sep. Purif. Technol.*, 2014, **123**, 130–138.

22 F. Shiraishi, A. Miyawaki and R. Chand, A mechanism of the photocatalytic decomposition of 2,4-dinitrophenol on TiO_2 immobilized on a glass surface, *Chem. Eng. J.*, 2015, **262**, 831–838.

23 T. T. Vu, T. Valdés-Solís and G. Marbán, High surface area stainless steel wire mesh-supported TiO_2 prepared by sacrificial template accelerated hydrolysis. A monolithic photocatalyst superior to P25 TiO_2, *J. Environ. Chem. Eng.*, 2014, **2**, 2229–2235.

24 Z. Wang, K. Yoshinaga, X. R. Bu and M. Zhang, Low temperature fabrication & photocatalytical activity of carbon fiber-supported TiO_2 with different phase compositions, *J. Hazard. Mater.*, 2015, **290**, 134–141.

25 D. Li, Q. Zhu, C. Han, Y. Yang, W. Jiang and Z. Zhang, Photocatalytic degradation of recalcitrant organic pollutants in water using a novel cylindrical multi-column photoreactor packed with TiO_2-coated silica gel beads, *J. Hazard. Mater.*, 2015, **285**, 398–408.

26 S. Singh, H. Mahalingam and P. K. Singh, Polymer-supported titanium dioxide photocatalysts for environmental remediation: a review, *Appl. Catal., A*, 2013, **462**, 178–195.

27 C. D. Tran, S. Duri, A. Delneri and M. Franko, Chitosan-cellulose composite materials: preparation, characterization and application for removal of microcystin, *J. Hazard. Mater.*, 2013, **252**, 355–366.

28 D. DelaiáSun, Facile fabrication of porous chitosan/TiO_2/Fe_3O_4 microspheres with multifunction for water purifications, *New J. Chem.*, 2011, **35**, 137–140.

29 P. Magesan, S. Sanuja and M. J. Umapathy, Novel hybrid chitosan blended MoO_3–TiO_2 nanocomposite film: evaluation of its solar light photocatalytic and antibacterial activities, *RSC Adv.*, 2015, **53**, 42506–42515.

30 C. D. Wagner, *Handbook of X-ray photoelectron spectroscopy: a reference book of standard data for use in X-ray photoelectron spectroscopy*, Physical Electronics Division, Perkin-Elmer Corp, 1979.

31 G. Xiao, H. Su and T. Tan, Synthesis of core–shell bioaffinity chitosan–TiO_2 composite and its environmental applications, *J. Hazard. Mater.*, 2015, **283**, 888–896.

32 S. Oros-Ruiz, R. Zanella and B. Prado, Photocatalytic degradation of trimethoprim by metallic nanoparticles supported on TiO_2-P25, *J. Hazard. Mater.*, 2013, **263**, 28–35.

33 B. Tanhaei, A. Ayati, M. Lahtinen and M. Sillanpää, Preparation and characterization of a novel chitosan/Al_2O_3/magnetite nanoparticles composite adsorbent for kinetic, thermodynamic and isotherm studies of methyl orange adsorption, *Chem. Eng. J.*, 2015, **259**, 1–10.

34 Z. Zainal, L. K. Hui, M. Z. Hussein and A. H. Abdullah, Characterization of TiO_2–chitosan/glass photocatalyst for the removal of a monoazo dye *via* photodegradation–adsorption process, *J. Hazard. Mater.*, 2009, **164**, 138–145.

35 W. J. Zhou, Y. H. Leng, D. M. Hou, H. D. Li, L. G. Li, G. Q. Li, H. Liu and S. W. Chen, Phase transformation and enhanced photocatalytic activity of S-doped Ag_2O/TiO_2 heterostructured nanobelts, *Nanoscale*, 2014, **6**, 4698–4704.

36 N. Wei, H. Cui, Q. Song, L. Zhang, X. Song, K. Wang, Y. Zhang, J. Li, J. Wen and J. Tian, Ag_2O nanoparticle/TiO_2 nanobelt heterostructures with remarkable photo-response and photocatalytic properties under UV, visible and near-infrared irradiation, *Appl. Catal., B*, 2016, **198**, 83–90.

37 W. Zhou, H. Liu, J. Wang, D. Liu, G. Du and J. Cui, Ag_2O/TiO_2 nanobelts heterostructure with enhanced ultraviolet and visible photocatalytic activity, *ACS Appl. Mater. Interfaces*, 2010, **2**, 2385–2392.

38 W. Zhou, Y. Leng, D. Hou, H. Li, L. Li, G. Li, H. Liu and S. Chen, Phase transformation and enhanced photocatalytic activity of S-doped Ag_2O/TiO_2 heterostructured nanobelts, *Nanoscale*, 2014, **6**, 4698–4704.

39 F. Chen, Z. Liu, Y. Liu, P. Fang and Y. Dai, Enhanced adsorption and photocatalytic degradation of high-concentration methylene blue on Ag_2O-modified TiO_2-based nanosheet, *Chem. Eng. J.*, 2013, **221**, 283–291.

40 H. Hua, Y. Xi, Z. Zhao, X. Xie, C. Hu and H. Liu, Gram-scale wet chemical synthesis of Ag_2O/TiO_2 aggregated sphere heterostructure with high photocatalytic activity, *Mater. Lett.*, 2013, **91**, 81–83.

41 W. Jiang, X. Wang, Z. Wu, X. Yue, S. Yuan, H. Lu and B. Liang, Silver Oxide as Superb and Stable Photocatalyst under Visible and Near-Infrared Light Irradiation and Its Photocatalytic Mechanism, *Ind. Eng. Chem. Res.*, 2015, **54**, 832–841.

42 D. Sarkar, C. K. Ghosh, S. Mukherjee and K. K. Chattopadhyay, Three dimensional Ag_2O/TiO_2 type-II (p–n) nanoheterojunctions for superior photocatalytic activity, *ACS Appl. Mater. Interfaces*, 2012, **5**, 331–337.